High-Resolution Manganese X-ray Fluorescence Spectroscopy. Oxidation-State and Spin-State Sensitivity

G. Peng,[†] F. M. F. deGroot,[‡] K. Hämäläinen,[Δ] J. A. Moore,[‖] X. Wang,[†] M. M. Grush,[†] J. B. Hastings,[§] D. P. Siddons,[§] W. H. Armstrong,[⊥] O. C. Mullins,[▽] and S. P. Cramer*[,†,‖]

Contribution from the Department of Applied Science, University of California, Davis, California 95616, Spectroscopy of Solids and Surfaces, University of Nijmegen, Toernooiveld, NL-6526 ED Nijmegen, The Netherlands, Department of Physics, University of Helsinki, Helsinki, Finland, National Synchrotron Light Source, Brookhaven National Laboratory, Upton, New York 11973, Energy and Environment Division, Lawrence Berkeley Laboratory, Berkeley, California 94720, Department of Chemistry, Boston College, Boston, Massachusetts 02140, and Schlumberger-Doll Research, Old Quarry Road, Ridgefield, Connecticut 06877

Received May 27, 1993. Revised Manuscript Received December 9, 1993[•]

Abstract: Kβ X-ray emission spectra have been recorded for Mn(II), Mn(III), and Mn(IV) compounds with a variety of ligands. The spectra have be interpreted and simulated as atomic multiplets perturbed by a crystal field. The X-ray fluorescence in this region, which results from 3p → 1s transitions, is split between a strong $K\beta_{1,3}$ region and a weaker Kβ′ satellite. For Mn(II) complexes, the Kβ′ region derives from final states with antiparallel net spins between the $3p^5$ hole and the $3d^5$ valence shell. The $K\beta_{1,3}$ region is dominated by spin-parallel final states. For octahedral high-spin Mn(II), Mn(III), and Mn(IV) complexes, the $K\beta_{1,3}$ peak position shifts to lower energy with increasing oxidation state. The Kβ′ feature is weaker and broader for the higher oxidation states, and it is almost unobservable for low-spin Mn(III). Kβ fluorescence is a good probe of Mn spin state and oxidation state. Spin-selective X-ray absorption near-edge spectra, taken by monitoring specific Kβ features, are illustrated. The potential for site-selective absorption spectroscopy, based on monitoring chemically sensitive Kβ features, is discussed.

Introduction

X-ray absorption spectroscopy, in both the X-ray absorption near-edge-structure (XANES) and extended X-ray absorption fine-structure (EXAFS) regions, is now a popular tool for electronic and molecular structure determination.[1] One limitation of the technique, as commonly practiced, is that the spectra represent an average over all the chemical forms of a given element in the sample.[2] This paper presents a variety of new manganese Kβ X-ray emission spectra, along with theoretical simulations. The observed chemical sensitivity of the emission suggests the possibility of selectively probing different metal spin or oxidation sites in a complex sample, by monitoring excitation spectra with high resolution.

Kβ spectra result from 3p → 1s transitions. Strong final-state 3p3d exchange coupling results in a sensitivity to the 3d population and to the relative spin orientation of the 3p and 3d electrons. Although chemical shifts in manganese emission spectra have been known for over half a century,[3] the high flux from present synchrotron radiation wiggler beamlines[4] allows much better spectra to be obtained. With a spherically bent crystal monochromator, Mn Kβ emission spectra with unsurpassed resolution can be obtained in minutes.[5,6]

To explore the potential bioiorganic and chemical applications of high-resolution fluorescence spectroscopy, we have systematically examined Kβ spectra for a variety of Mn compounds. The new Kβ fluorescence spectra have been interpreted using atomic multiplet theory with the inclusion of an adjustable crystal field (ligand field multiplet calculations). These simulation procedures, initially developed for the interpretation of soft X-ray absorption spectra by Thole *et al.*,[7-10] can also explain the essential features of the emission spectra. Although additional work is needed to reproduce the spectra of the more covalent compounds, site-selective excitation spectroscopy using high-resolution fluorescence detection appears promising.

Experimental Section

Data Collection. The Kβ X-ray emission spectra were recorded on wiggler beamlines X-25[4] and X-21 at the National Synchrotron Light Source. On X-25, the synchrotron radiation was monochromated for 6.6-keV excitation energy using a pair of Si(220) crystals and focused to a submillimeter spot. For the X-21 experiments, sagitally focused 14-keV X-rays from a bent Si(220) crystal were used for excitation. The X-ray spectrometer used to disperse the Mn fluorescence employed a spherically bent Si(440) crystal in an apparatus that has been previously described.[6] A position-sensitive proportional chamber was used both for initial alignment and for fluorescence detection on beamline X-25. On beamline X-21, once the position and focus of the diffracted fluorescence

[†] University of California.
[‡] University of Nijmegen.
[Δ] University of Helsinki.
[§] Brookhaven National Laboratory.
[‖] Lawrence Berkeley Laboratory.
[⊥] Boston College.
[▽] Schlumberger-Doll Research.

• Abstract published in *Advance ACS Abstracts*, February 1, 1994.

(1) *X-ray absorption: principles, applications, techniques of EXAFS, SEXAFS, and XANES*; Koningsberger, D. C., Prins, R., Eds.; Wiley: New York, 1988.

(2) Chemically selective XAS using soft X-ray fluorescence has been discussed previously: Stöhr, J. *NEXAFS Spectroscopy*; Springer-Verlag: New York, 1992.

(3) Sanner, V. H. Ph.D. Thesis, University of Uppsala, 1941.

(4) Berman, L. E.; Hastings, J. B.; Oversluizen, T.; Woodle, M. *Rev. Sci. Instrum.* **1992**, *63*, 428.

(5) (a) Hämäläinen, K.; Kao, C. C.; Hastings, J. B.; Siddons, D. P.; Berman, L. E.; Stojanoff, V.; Cramer, S. P. *Phys. Rev. B.* **1992**, *46*, 14274. (b) Hämäläinen, K.; Siddons, D. P.; Hastings, J. B.; Berman, L. E. *Phys. Rev. Lett.* **1991**, *67*, 2850.

(6) Stojanoff, V.; Hämäläinen, K.; Siddons, D. P.; Hastings, J. B.; Berman, L. E.; Cramer, S. P.; Smith, G. *Rev. Sci. Instrum.* **1992**, *63*, 1125–1127.

(7) Thole, B. T.; Cowan, R. D.; Sawatzky, G. A.; Fink, J.; Fuggle, J. C. *Phys. Rev. B* **1985**, *31*, 6856.

(8) Thole, B. T.; van der Laan, G.; Fuggle, J. C.; Sawatzky, G. A.; Karnatak, R. C.; Esteve, J.-M. *Phys. Rev. B* **1985**, *32*, 5107.

(9) deGroot, F. M. F.; Fuggle, J. C.; Thole, B. T.; Sawatzky, G. A. *Phys. Rev. B* **1990**, *41*, 928.

(10) van der Laan, G.; Kirkman, I. W. *J. Phys. Condens. Matter* **1992**, *4*, 4189.

0002-7863/94/1516-2914$04.50/0

Scheme 1. Single-Particle Picture of Kβ Fluorescence

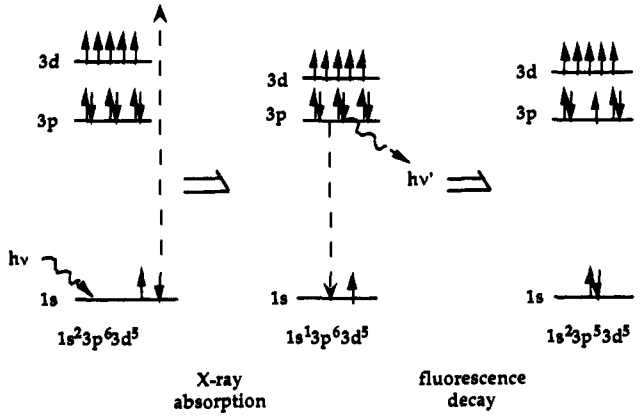

beam were confirmed with the position-sensitive detector, a small NaI detector was used for emission detection, with a slit to define the emission energy. The slit and detector were scanned horizontally to track the beam as the diffraction angle was changed by rotating the Si crystal.

During the X-25 experiments, the finely powdered compounds were mixed with a small amount of acetone-diluted Duco cement. The slurry was layered into a cylindrical depression to form a solid pellet, and the spectra were recorded at 20 K by using a liquid-helium refrigerator. During the X-21 experiments, the powdered samples were packed into a depression in a Lucite sample holder, and the measurements were taken at room temperature. On both beamlines, the spectra were calibrated by reference to the spectrum of Mn metal. An absolute energy for the main peak ($K\beta_{1,3}$) was obtained by measuring the diffraction angle, combined with Bragg's law and the known 1.92-Å Si(440) 2d spacing. This yielded an energy of 6490.0 eV for the Mn metal ($K\beta_{1,3}$) peak. From the number of steps taken by the emission monochromator, other absolute angles and energies were calibrated. The calibrated was periodically checked and adjusted by measuring an MnF_2 sample, with the $K\beta_{1,3}$ peak assigned as 6491.7 eV.

Samples. MnF_2, $MnCl_2$, $Mn(OAc)_2$, and $Mn(OAc)_3$ were used as received from Aldrich. Mn(P)Cl was used as received from Midcentury. $[HB(3,5\text{-}Me_2pz)_3]_2Mn(ClO_4)_2$,[11] $(NEt_4)_2MnCl_4$,[12] $[HB(3,5\text{-}Me_2pz)_3]_2Mn(ClO_4)$,[13] $[HB(3,5\text{-}Me_2pz)_3]_2Mn$,[13] and Mn(acen)Cl[14] were prepared in the Armstrong laboratory by the cited literature methods. $Mn[B(3\text{-}Ph\text{-}pz)_4]_2$ was prepared in the McKee laboratory.[15] $Mn_2O_2(pic)_4$[16] was prepared in the Christou laboratory. $Mn(phen)Cl_3$[17] and $K_3Mn(CN)_6$[18] were prepared in the Cramer laboratory.[19]

Theory

Initially, a single-particle picture (Scheme 1) will be used to describe the Kβ fluorescence process, using the high-spin Mn(II) case as an example. In the ground state, the 3d orbitals are filled with five spin-up electrons at an orbital energy e_d (neglecting ligand field effects for the moment). The completely filled band formed by the ligand p orbitals has an energy e_p. In K-shell absorption, a 1s electron is ejected and a 1s core hole is created. When a 3p electron relaxes to the 1s core hole, Kβ fluorescence is emitted, and a final state with a hole in the 3p shell is reached. The strong coupling between the 3p core hole and the partially filled 3d orbitals yields atomic multiplets which are spread over a 15-eV energy range. Tsutsumi and co-workers interpreted the fluorescence spectra in terms of the exchange interaction of the 3p hole with the partially filled 3d shell in the final state.[20,21]

Table 1. $K\beta_{1,3}$ and Kβ′ Peak Positions of the Mn Kβ Emission Spectra Recorded at 297 K (Accuracy ±0.2 eV)

compound	polyhedra	position (eV) $K\beta_{1,3}$	position (eV) Kβ′
Manganese(II)			
MnF_2	$[MnF_6]$	6491.7	6474.8
$Mn(OAc)_2$	$[MnO_6]$	6491.5	6475.2
$Mn[HB(3,5\text{-}Me_2pz)_3]_2$	$[MnN_6]$	6491.4	6475.3
$MnCl_2$	$[MnCl_6]$	6491.3	6474.9
$(Et_4N)_2MnCl_4$	$[MnCl_4]$	6491.0	6475.5
Manganese(III)			
$Mn(phen)Cl_3$	$[MnN_2Cl_3]$	6490.9	6475.7
$Mn(OAc)_3$	$[MnO_6]$	6490.8	6475.6
Mn(P)Cl	$[MnN_4Cl]$	6490.6	6475.7
Mn(acen)Cl	$[MnN_4Cl]$	6490.4	6475.8
$Mn[HB(3,5\text{-}Me_2pz)_3]_2(ClO_4)$	$[MnN_6]$	6489.6	
K_3MnCN_6	$[Mn(CN)_6]$	6489.4	
Manganese(IV)			
$Mn[HB(3,5\text{-}Me_2pz)_3]_2(ClO_4)_2$	$[MnN_6]$	6490.3	
$Mn_2O_2(pic)_4$	$[MnN_2O_4]$	6490.6	

They were able to calculate the splitting between the $K\beta_{1,3}$ line (the strongest Kβ feature) and the Kβ′ satellite line (a weaker peak or shoulder at lower energies), as well as the ratio of peak intensities.[22] In the ligand field atomic multiplet model, we account for the effective exchange splitting as well as all possible couplings of the angular momenta. Our results are consistent with the Tsutsumi assignments, and some additional features are explained.

Assuming that Mn(II) with a $1s^23p^63d^5$ configuration has a weak charge-transfer effect, it is reasonable to take the $|1s^13p^63d^5\rangle$ configuration as the intermediate state of the Kβ fluorescence process (see Appendix). Charge-transfer effects can be taken into account by a reduction of the Slater integrals in the calculation, thereby simulating the changes in the radial part of the wave functions.[23]

Our calculations for the fluorescence process take into account the total symmetry for the intermediate state, namely the [5S] and [7S] symmetries which come from coupling the 1s core electron with the $3d^5$ electrons, $[^{5,7}S \equiv {}^6S \otimes {}^2S]$. From the dipole transition selection rules the final states will have ^5P or ^7P symmetry. These result from the two possible spin orientations for the 3p hole, spin-up or spin-down, with respect to the shell of spin-up d electrons. In the spin-down hole case, the net 3p electron spin couples with the five spin-up 3d electrons and gives a lower energy ^7P term (higher energy fluorescence), while spin-up yields ^5P. The energy difference between the ^7P and ^5P terms is the exchange splitting from 3p3d exchange interactions. Additional splittings from the cubic crystal field, from 3d spin–orbit coupling, and from Jahn–Teller distortions are also included in the ligand field atomic multiplet calculations.

The parameters used in the calculations are therefore the 3p3d Slater integrals (Coulomb and exchange integrals F^2_{pd}, G^1, and G^3), the 3d3d Slater integrals (F^2_{dd} and F^4_{dd}), and the 3p (ξ_{3p}) as well as 3d (ξ_{3d}) spin–orbit couplings. The atomic values for the Slater integrals were calculated within the Hartree–Fock limit.[24] The Hartree–Fock values were reduced to 80% to account for configuration interaction effects.[24] The calculated spectral lines were convoluted with a Lorentzian to reflect lifetime broadening and with a Gaussian to account for experimental broadening. The calculations were not used to obtain absolute energies; the calculated spectra were arbitrarily shifted along the energy axis to align with experimental spectra.

(11) Chan, M. K.; Armstrong, W. H. *Inorg. Chem.* **1989**, *28*, 3777.
(12) Gill, N. S.; Taylor, F. B. *Inorg. Synth.* **1967**, *9*, 136.
(13) Chan, M. K.; Armstrong, W. H. Manuscript in preparation.
(14) Boucher, L. J.; Day, V. W. *Inorg. Chem.* **1977**, *16*, 1360.
(15) Brooker, S.; McKee, V. *J. Chem. Soc., Chem. Commun.* **1989**, 619.
(16) Christou, G. *Acc. Chem. Res.* **1989**, *22*, 328–335.
(17) *Gmelins Handbuch der Anorganischen Chemie*; Springer-Verlag: Berlin, 1982; Vol. D3, pp 201, 241.
(18) Traggeser, G.; Eysel, H. H. *Inorg. Nucl. Chem. Lett.* **1978**, *14*, 65.
(19) Abbreviations used: acen, *N,N'*-ethylenebis(acetylacetone imine); pic, picolinate anion; P, protoporphyrin IX; OAc, acetate; pz, pyrazole; phen, phenanthroline.
(20) Tsutsumi, K. *J. Phys. Soc. Jpn.* **1959**, *14*, 1696.
(21) Tsutsumi, K. Nakamori, H. *J. Phys. Soc. Jpn.* **1968**, *25*, 1418.
(22) Tsutsumi, K. Nakamori, H.; Ichikawa, K. *Phys. Rev. B.* **1976**, *13*, 929.
(23) deGroot, F. M. F. Ph.D. Thesis, University of Nijmegen, 1991.
(24) Cowan, R. D. *The Theory of Atomic Structure and Spectra*; University of California Press: Berkeley, CA, 1981; p 464.

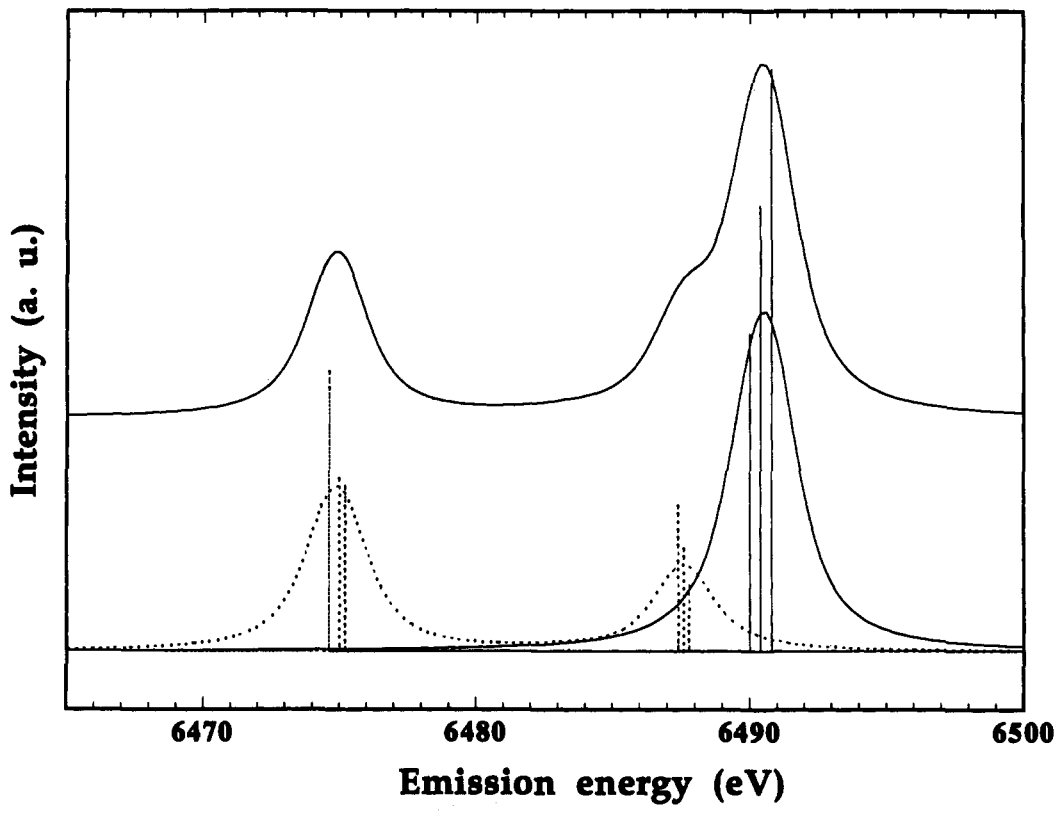

Figure 1. Atomic multiplet calculation for the $1s^13p^63d^5 \rightarrow 1s^23p^53d^5$ transitions of Mn(II). Bottom: Calculated spectra for $^7P_{4,3,2}$ (—) and the $^5P_{3,2,1}$ (···) final states. The sticks indicate the energy positions and relative intensities of all allowed dipole transitions, and the curves are the broadened spectra. Top: Sum of the $^7P_{4,3,2}$ and the $^5P_{3,2,1}$ spectra. A Lorentzian broadening of 1.0 eV was used as well as a Gaussian broadening of 0.5 eV. The energy scale was shifted to agree with experimental values.

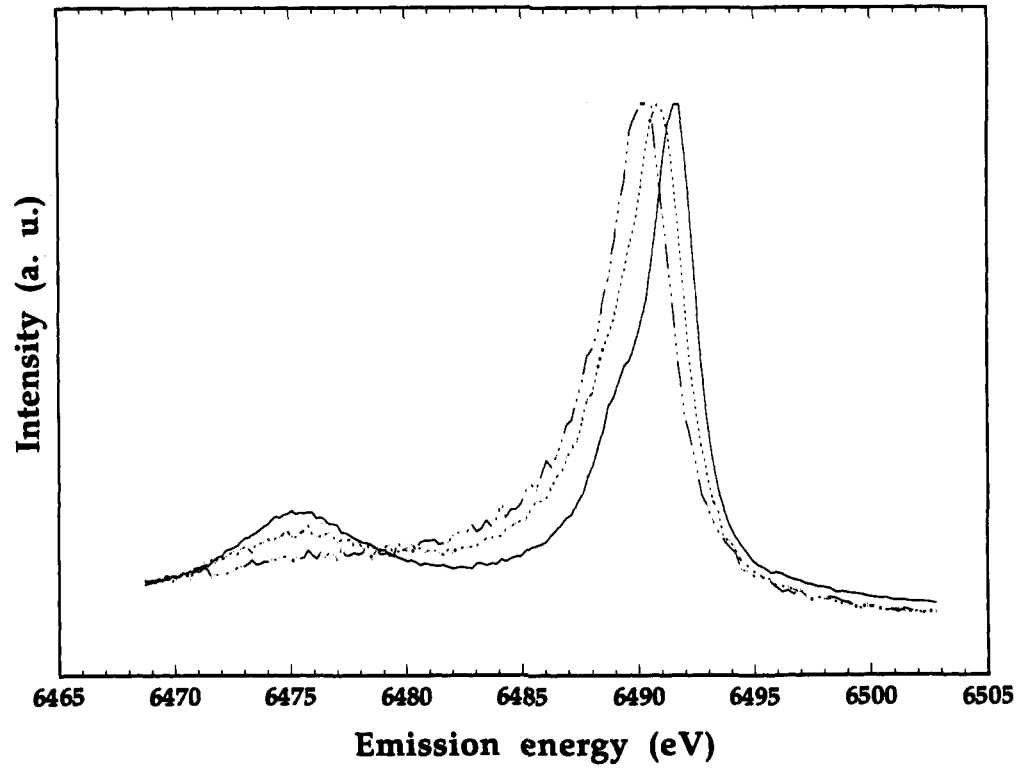

Figure 2. Oxidation-state effects on peak shapes and positions for Mn Kβ spectra: $Mn^{II}(OAc)_2$ (—); $Mn^{III}(OAc)_3$ (- - -); $Mn^{IV}[HB(3,5\text{-}Me_2pz)_3]_2(ClO_4)_2$ (- - - - -).

Figure 1 illustrates the results of the atomic multiplet calculation for Mn^{2+}. The calculation confirms that the main features of the $K\beta_{1,3}$ and $K\beta'$ regions correspond respectively to transitions to ^7P and ^5P final states. The 3p3d exchange interaction splits these two ^7P and ^5P terms by 16 eV. The 3p spin–orbit coupling further splits both of these terms into $^7P_{4,3,2}$ and $^5P_{3,2,1}$ levels, with splitting on the order of 1 eV. The individual transitions have intensity ratios of 9:7:5 and 7:5:3, respectively.

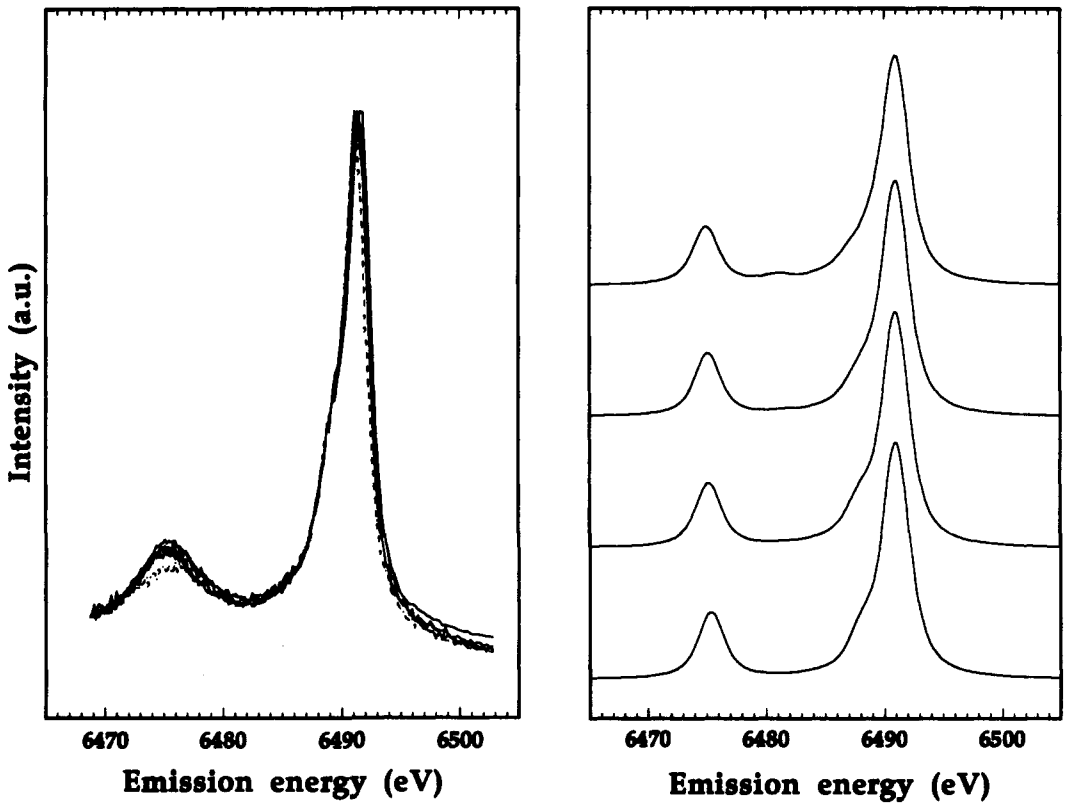

Figure 3. Left: Experimental ligand field effects on Mn(II) Kβ spectra. Key: $MnCl_2$, $Mn[HB(3,5\text{-}Me_2pz)_3]_2$, $Mn(OAc)_2$, and $Mn[B(3\text{-}Ph\text{-}pz)_4]_2$ superimposed (—); $MnCl_4^{2-}$ (···). Right: Calculated ligand field effects on Mn(II) Kβ spectra. Top to bottom: spectra for $10Dq$ = 3, 1.8, 1.2, and 0 eV. For the calculated spectra, a Lorentzian broadening of 1.0 eV was used as well as a Gaussian broadening of 0.5 eV.

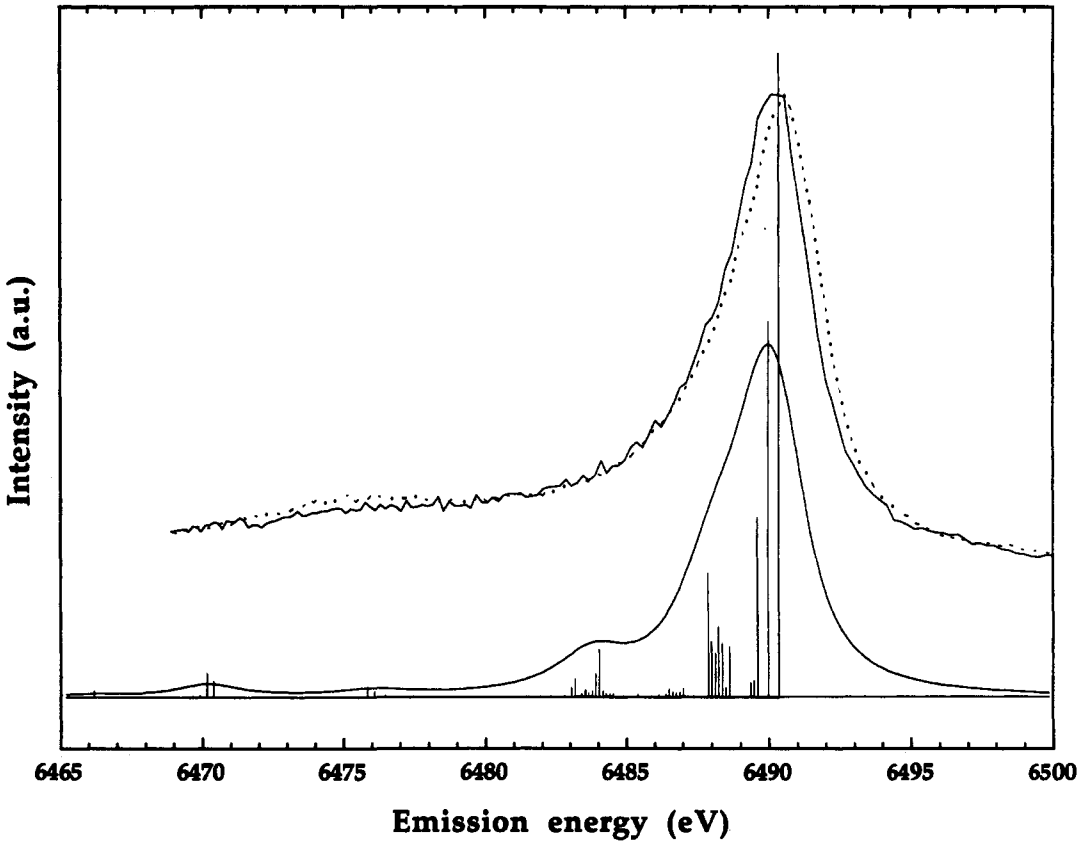

Figure 4. Comparison of experimental and theoretical spectra of Mn(IV) compounds. Top: Experimental spectra for $Mn^{IV}[HB(3,5\text{-}Me_2pz)_3]_2(ClO_4)_2$ (—) and $Mn_2O_2(pic)_4$ (···). Bottom: Calculated spectrum with a Lorentzian broadening of 1.0 eV and a Gaussian broadening of 0.5 eV. The sticks indicate the energy positions and relative intensities of all allowed dipole transitions.

An additional term in the calculation at the low-energy side of the $K\beta_{1,3}$ peak has ^5P symmetry (the ^5P shoulder) and involves final states with one spin-down 3p hole coupled with four spin-up and one spin-down 3d electrons. This term has an energy close

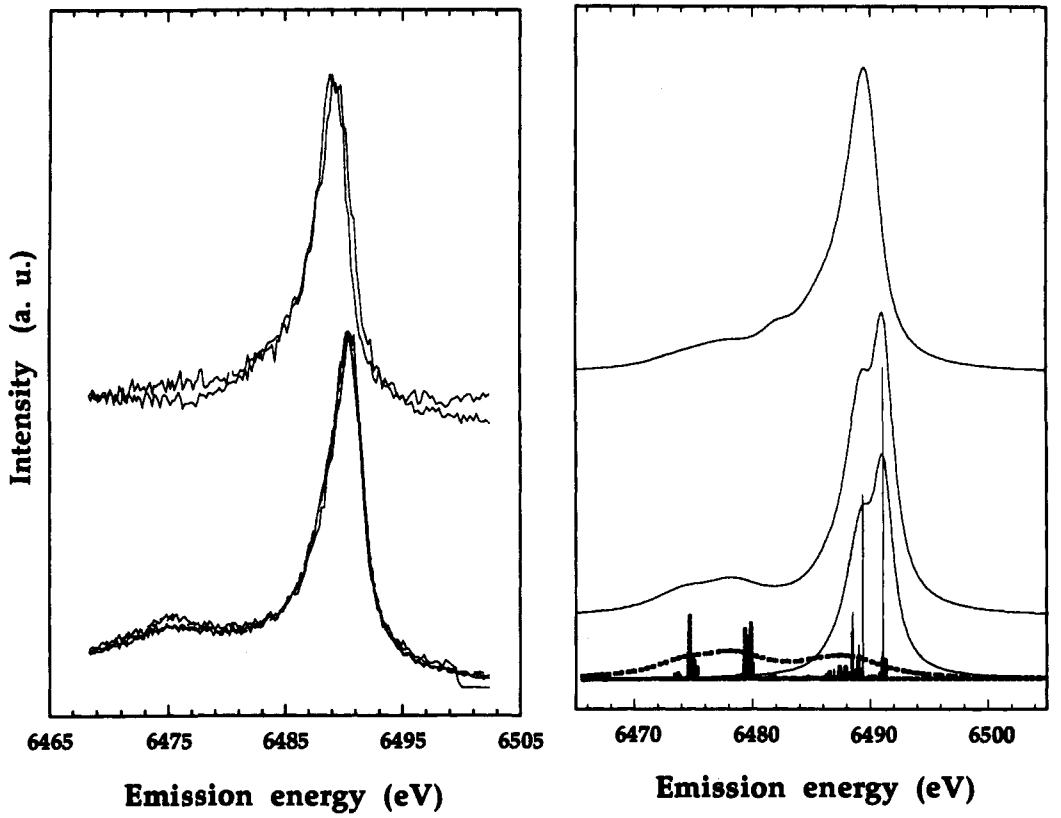

Figure 5. Left: Spectra of a representative series of Mn(III) compounds with different spin states. Key: top, low-spin $K_3Mn(CN)_6$ and $Mn[HB(3,5\text{-}Me_2pz)_3]_2(ClO_4)$; bottom, high-spin $Mn(OAc)_3$, Mn(acen)Cl, Mn(P)Cl, and Mn(phen)Cl_3. Right: Calculated spectra of low spin (top) vs high-spin compounds (middle). Bottom spectra are the calculated spectra for $^7P_{4,3,2}$ (—) and $^5P_{3,2,1}$ (- - -) final states, which give the middle summation spectrum. The calculated spectra are broadened with Lorentzian broadenings of 1.0 eV for the $K\beta_{1,3}$ structure and 2.0 eV for the $K\beta'$ as well as a Gaussian broadening of 0.5 eV.

to the ^7P-symmetry transitions, because both final states contain a spin-up 3p electron. The 3d3d exchange coupling causes the energy difference between this ^5P shoulder and the ^7P term.

Results and Discussion

The $K\beta$ X-ray emission spectra of a series of Mn compounds with the same geometry and different oxidation states are shown in Figure 2 and summarized in Table 1. The spectral shape and position vary with the spin state and oxidation state of Mn. The octahedral Mn(II) compounds show a $K\beta_{1,3}$ peak near 6491.5 eV, a $K\beta'$ peak 16 eV lower, and a weak shoulder on the low-energy side of the $K\beta_{1,3}$ peak. The $K\beta_{1,3}$ centroid is shifted ~0.7 eV to lower energy for high-spin Mn(III), and an additional 0.5-eV shift is observed for Mn(IV). The spectra of the Mn(III) and Mn(IV) compounds are broader and have less intensity in the $K\beta'$ satellite region. This same trend for manganese compounds has been observed previously at low resolution for low-spin Mn(III).[25]

Mn(II) Spectra. The spectra for several high-spin Mn(II) complexes are shown in Figure 3; there is little variation in spectral shape. The $K\beta'$ satellite has slightly more intensity for all Mn compounds with O_h symmetry than for tetrahedral $MnCl_4^{2-}$, and the shoulder of the $K\beta_{1,3}$ peak shows a small increase in intensity with stronger crystal fields. This relative insensitivity of the spectra to ligand field is also found in the theoretical simulations. The $K\beta$ spectra are simulated with the $1s^13d^5\,^6S$ initial state and $^7P_{4,3,2}$ and $^5P_{3,2,1}$ final states. A cubic crystal field splits the 3d states into a triplet of T_2 symmetry and a doublet of E symmetry but does not affect the total energy for the ^7P term or for the ^5P $K\beta'$ region. The other ^5P term, the shoulder ^5P on the low-energy side of the ^7P term, has one spin-down and four spin-up 3d electrons, and the ligand field does split this term. Therefore, only the shoulder ^5P feature is directly sensitive to the ligand field. A comparison of ligand field atomic multiplet calculations with the experimental results is shown in Figure 3.

Mn(IV) Spectra. Spectra for two Mn(IV) compounds with O_h geometries are shown in Figure 4. A $K\beta_{1,3}$ peak is seen at about 6490.5 eV, with a shoulder on the low-energy side, but the $K\beta'$ peak is not clearly observable. The fluorescence spectra were simulated with a $3d^3$ $[^4A_2]$ ground state and a $1s^13d^3$ intermediate state. The experimental and theoretical spectra agree on the weakness of the $K\beta'$ peak and the general shape of the main peak. Analysis of calculations for many possible transitions reveals that a large number of $3p^53d^3$ states are symmetry-allowed final states, especially in the case of a strong crystal field. The weakness of the $K\beta'$ peak may result from experimental broadening of this large number of low-intensity peaks, as seen by the many transitions in the energy range 6465–6485 eV. The absence of the extra calculated peak at 6484 eV in the experimental spectra may come from the increased covalency of Mn(IV).

Mn(III) Spectra. The Mn(III) compounds studied were Mn(OAc)$_3$, Mn(acen)Cl, Mn(P)Cl, Mn(phen)Cl_3, K_3MnCN_6, and $Mn[HB(3,5\text{-}Me_2pz)_3]_2(ClO_4)$. They can be grouped into two groups: low-spin $3d^4$ compounds, μ_{eff} = 3.1–3.2 μ_B, and high-spin $3d^4$, μ_{eff} = 4.8–5.3 μ_B. $Mn[HB(3,5\text{-}Me_2pz)_3]_2(ClO_4)$ and $K_3Mn(CN)_6$ belong to the first group, and the rest of the Mn(III) compounds belong to the second.[26] The spectra of high-spin Mn(III) compounds have the $K\beta_{1,3}$ peak centered at ~6490.7 eV, and the $K\beta'$ peak sits at 16 eV lower energy (Figure 5, left). The spectra of low-spin Mn(III) compounds have the $K\beta_{1,3}$ peak near ~6489.5 eV and no distinct $K\beta'$ peak.

(25) Urch, D. S.; Wood, P. R. *X-ray Spectrom.* **1978**, *7*, 9.

(26) Chiswell, B.; McKenzie, E. D.; Lindoy, L. F. In *Comprehensive Coordination Chemistry*; Wilkson, S. G., Ed.; Pergamon Press: New York, 1987; Chapter 41.

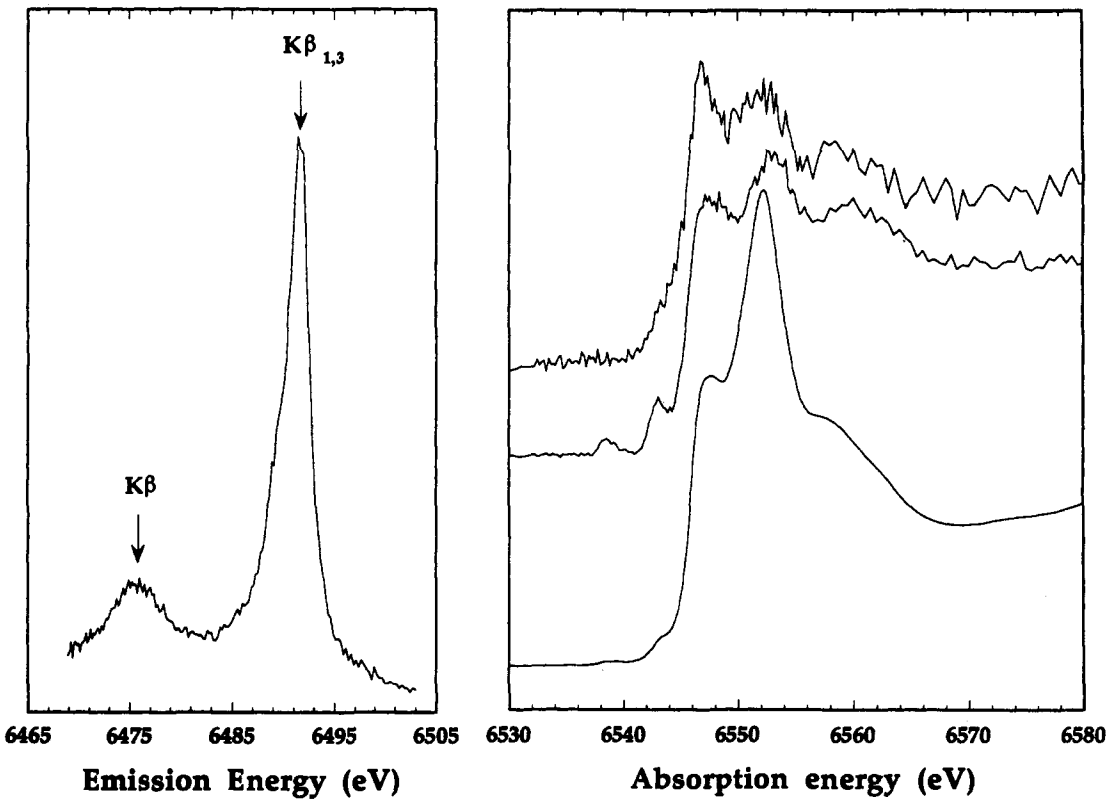

Figure 6. Spin-selective study of $[HB(3,5\text{-}Me_2pz)_3]_2Mn^{II}$. Left:' Kβ emission spectrum illustrating the selected emission energies. Right: XANES spectra for spin-up states acquired by monitoring emission at the Kβ′ peak energy (top) and for spin-down states acquired by monitoring emission at the $K\beta_{1,3}$ peak energy (middle); the normal K-edge transmission spectrum (bottom).

A comparison between experimental and calculated spectra for both high-spin and low-spin Mn(III) is shown in Figure 5. Mn(III) Kβ emission spectra are described as $1s^13p^63d^4 \rightarrow 1s^23p^53d^4$ transitions. This ion is especially interesting because of the more frequent occurrence of both high-spin and low-spin compounds and the Jahn–Teller distortions of the former. Low-spin Mn(III) has $^3T_1$ symmetry for the d orbitals which will be affected by the 3d spin–orbit coupling.[27] Spin–orbit coupling will mix the high-spin into a low-spin state and results in a intermediate effective spin value. In this work, we used the pure spin state as the ground state to simplify the situation. For the low-spin Mn(III) spectra, the agreement between experiment and calculations is reasonable.

The calculations for high-spin Mn(III) spectra have been improved by applying Jahn–Teller distortions in the calculation, from O_h to D_{4h} with splitting between $d_{x^2-y^2}$ and d_{z^2} ($D_s = -358$ meV). The disagreement between experiment and calculations may result from the range of possible initial states, 3d spin–orbit coupling, covalency, and/or charge transfer. Study of the 3d spin–orbit coupling effects reveals that they correlate with the crystal field strength. A detailed study of the charge-transfer effects and covalence would require using a more comprehensive theory, e.g. the configuration interaction cluster model which accounts both for multiplets and charge transfer.

Spin-Selective Excitation Spectroscopy. For Mn(II) compounds, $K\beta_{1,3}$ and Kβ′ correspond to spin-down and spin-up holes in the $3p^53d^5$ final state, respectively. Near the $K\beta_{1,3}$ peak energy, more than 90% of the emission derives from a 3p spin-down hole final state, while at the Kβ′ peak energy, 100% of the emission results from a 3p spin-up hole. The clear separation between these two features allows the possibility of spin-selective measurements of the K-edge X-ray absorption spectrum.[5]

(27) Griffith, J. S. *The Theory of Transition Metal Ions*; University Press: Cambridge, U.K., 1964; Chapter 9.

Spin-selective excitation spectra for $Mn[HB(3,5\text{-}Me_2pz)_3]_2$ have been recorded (Figure 6). At the foot of the K absorption edge, 1s → 3d transitions are observed near 6540 eV. For this high-spin Mn(II) complex, the spin-up 3d states are all occupied. Therefore, the 1s → 3d transition is not allowed for a spin-up electron and should be absent in the X-ray absorption spectrum when Kβ′ is monitored. Indeed, the 1s → 3d features are absent from the Kβ′ excitation spectrum. For excitation spectra that monitor the $K\beta_{1,3}$ peak, the situation is reversed. Transitions for a spin-down electron to the 3d band are theoretically allowed, and since these give rise to $K\beta_{1,3}$ emission, 1s → 3d transitions are experimentally observed in the excitation spectrum. Additional differences at the higher energies are also seen, but not yet interpreted. These high-resolution excitation spectra also show line-sharpening effects, which have been discussed by Hämäläinen *et al.*[5]

Conclusions

We have shown that the $K\beta_{1,3}$ peak position and Kβ′ peak intensity depend notably both on the oxidation state of Mn and on the spin state of Mn. The average energy of the $K\beta_{1,3}$ feature shifts to lower energy by ~0.7 eV between Mn(II) and Mn(III) and a smaller shift between Mn(III) and Mn(IV) for high-spin Mn. The Kβ′ peak intensity decreases as the formal charge on Mn increases from Mn(II) to Mn(III) to Mn(IV). The $K\beta_{1,3}$ peak positions are separated by ~0.8 eV for different spin states of Mn(III). The Kβ spectra of Mn(II) compounds have been explained in detail, using multiplet calculations for $1s^13p^63d^5 \rightarrow 1s^23p^53d^5$ transitions. For formally Mn(IV) compounds, the weakness of Kβ′ has been observed by experiments and interpreted by the theory. For Mn(III) compounds, both experiment and theory found a Kβ′ satellite for the high-spin compounds which disappeared for low-spin compounds. Compared with the substantial changes with oxidation state and spin state, the spectral shape variations with crystal field strength are small. The weak

dependency on crystal field strength makes it difficult to accurately determine crystal field strengths from Kβ fluorescence.

The atomic multiplet calculations including an adjustable crystal field reproduce the spectral shape of Kβ emission spectra. The symmetry of the ground state is the crucial factor, and it determines the actual spectral shape, despite changes in the electronic configuration due to charge transfer after core hole creation. For the higher oxidation states, the precise spectral shape is less accurately reproduced.

The strong 3p3d exchange coupling allows measurement of spin-polarized K-edge X-ray absorption spectra, and this has been demonstrated for Mn(II). By monitoring specific fluorescence energies, it should also be possible to perform oxidation-state-specific EXAFS experiments. Oxidation-state- and spin-selective excitation spectroscopy will be useful for probing specific sites in mixed-valence systems, thus overcoming one of the major limitations of the EXAFS technique.

Acknowledgment. We thank Dr. J. van Elp (LBL) for useful discussions, Professor G. Christou (Indiana University) for $Mn_2O_2(pic)_4$, and Professor V. McKee (University of Christchurch) for $Mn[B(3\text{-}Ph\text{-}pz)_4]_2$. This work was supported by the National Institutes of Health, Grant GM-48145 (S.P.C.), by the ACS Petroleum Research Fund, and by the Department of Energy, Office of Health and Environmental Research. W.H.A. acknowledges funding from the National Institutes of Health, Grant GM-38275, and from the Searle Scholars and the National Science Foundation Presidential Young Investigators Programs. The National Synchrotron Light Source is funded by the Department of Energy, Office of Basic Energy Research.

Appendix

In describing the multiplet effects, we have to consider the possibility of charge transfer (Scheme 2). It has been argued for Ni(II) that the $3p^53d^9\underline{L}$ (where $\underline{L}$ represents a ligand hole) multiplet largely determines the Kβ spectral shape,[28] and charge transfer is also very important for 2p XPS of Ni compounds.[29] The ground state for Mn(II) has a $|1s^23p^63d^5\rangle$ configuration with ^6S symmetry. The charge-transfer state with $|1s^23p^63d^6\underline{L}\rangle$

(28) Kawai, J.; Takami, M.; Satoko, C. *Phys. Rev. Lett.* **1990**, *65*, 2193.
(29) Zaanen, J.; Westra, C.; Sawatzky, G. A. *Phys. Rev. B.* **1986**, *33*, 4369.

Scheme 2. Possible Charge-Transfer Effects during Kβ Fluorescence

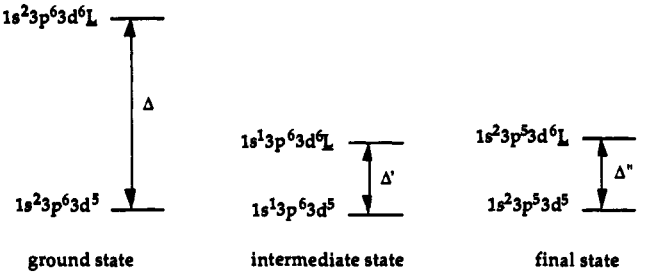

configuration (one ligand electron hops to a 3d orbital) is shifted by an energy $\Delta = e_d - e_p$ but has the same ^6S total symmetry. So the ground state with charge-transfer effect is a mixture of $|1s^23p^63d^5\rangle$ and $|1s^23p^63d^6\underline{L}\rangle$ ($\alpha|1s^23p^63d^5\rangle + \beta|1s^23p^63d^6\underline{L}\rangle$) with ^6S symmetry. After X-ray absorption, a 1s core hole is created, which changes the energies of both configurations because of the 1s–3d Coulomb interaction. This pulls the $|1s^13p^63d^6\underline{L}\rangle$ intermediate state further down as compared to $|1s^13p^63d^5\rangle$. As a result of this Coulomb interaction, the intermediate state levels are now closer together ($0 < \Delta' < \Delta$) or even inverted ($\Delta' < 0$). The intermediate state will be $\alpha'|1s3p^63d^5\rangle + \beta'|1s3p^63d^6\underline{L}\rangle$ with $^{5,7}S$ symmetry. After Kβ decay, the 1s core hole is filled with an electron from the 3p level. In the final states, we have Coulomb and exchange interactions between the 3p core hole and the 3d electrons. The final state will be of $\alpha''|1s^23p^53d^5\rangle + \beta''|1s^23p^53d^6\underline{L}\rangle$ character.

The fluorescence transition probability is determined by the Fermi's Golden rule for dipole transitions. Because the core potential of a 1s core hole is similar to that of the 3p core hole, we expect no major charge-transfer effect to occur in the fluorescence process. The transition probabilities for both $\alpha'|1s^13p^63d^5\rangle + \beta'|1s^13p^63d^6\underline{L}\rangle$ and $|1s^13p^63d^5\rangle$ are similar to those for their final states. If we assume that the final-state energy differences for $\alpha''|1s^13p^63d^5\rangle + \beta''|1s^13p^63d^6\underline{L}\rangle$ and $|1s^13p^63d^5\rangle$ are similar ($\Delta'' \sim \Delta'$), then we can describe the Kβ fluorescence process by using a ligand field atomic multiplet model starting from a $|1s^13p^63d^5\rangle$ intermediate state and going to $|1s^23p^53d^5\rangle$.